J. Fluid Mech. (2005), *vol.* 528, *pp.* 207–232.
doi:10.1017/S002211200400326X Printed in the United Kingdom

On the role of non-equipartition in the dynamics of rapidly flowing granular mixtures

By J. E. GALVIN, S. R. DAHL AND C. M. HRENYA†

Department of Chemical and Biological Engineering, University of Colorado, Boulder, CO 80309, USA

(Received 20 August 2002 and in revised form 8 November 2004)

For rapidly flowing granular mixtures, existing kinetic-theory descriptions based on an assumed form of the velocity distribution function typically contain one of two simplifying assumptions: a Maxwellian velocity distribution or an equipartition of energy. In the current work, the influence of non-equipartition effects is explored in the context of two flow types: flow in which species segregation does not occur (namely, simple shear flow) and a segregating flow. For the former case, a comparison between existing kinetic theories and molecular-dynamics simulations of a binary system indicates that the incorporation of a non-Maxwellian velocity distribution is critical for reliable stress predictions, as is consistent with previous findings. However, the predictions are fairly insensitive to the equipartition versus non-equipartition treatment, despite the presence of a significant non-equipartition of energy. Nevertheless, an analysis of the diffusion equation for a segregating flow indicates that the presence of a non-equipartition of energy gives rise to additional components of the driving forces associated with size segregation. These additional components involve gradients of the species temperature, whereas theories based on an equipartition assumption only involve gradients in the mixture temperature. Molecular-dynamics simulations of the segregating flow, in conjunction with kinetic theory of binary systems, show that the non-equipartition effects are non-negligible for systems characterized by moderate values of mass differences and restitution coefficients. These simulations also reveal that the more massive particle may exhibit a lower species temperature than its lighter counterpart, contrary to previous observations in non-segregating systems. A physical explanation for this behaviour is provided.

1. Introduction

Flows composed of solid particulates occur in a wide variety of industrial, geophysical, and astrophysical systems, including solids mixers and hoppers, chute flows, landslides, avalanches and planetary rings. The granular medium is often composed of grains which differ in size and/or material density. Such particle non-uniformity is expected to lead to a bulk flow behaviour which is different from that for a medium composed of identical particles. In addition, a phenomenon unique to particle mixtures (i.e. media composed of non-identical particles) may also occur, namely the segregation of unlike particles. Although this segregation phenomenon may be capitalized upon for applications in which a separation of unlike particles is desired (e.g. mining), such segregation may prove detrimental for systems in which a

† Author to whom correspondence should be addressed: hrenya@colorado.edu

uniform blend is desired (e.g. mixing of pharmaceutical powders). (For overviews of mixing and segregation, see Savage 1987; Bridgwater 1994; Ottino & Khakhar 2000; Rosato & Blackmore 2000).

In the current work, attention is paid to granular mixtures engaged in rapid flow, which is characterized by nearly instantaneous interactions between particles (unlike the slow-flow regime, which is typified by enduring contacts between particles). The most sophisticated continuum models available to describe such flows are derived from dense-gas kinetic theory, with a modification to account for the presence of inelastic collisions between particles. (For reviews of kinetic-theory models, see Campbell 1990; Ernst 2000; Goldhirsch 2003) Generally speaking, the mixture models involve the solution of a mass and momentum balance for each species i:

$$\frac{\partial \rho_i}{\partial t} + \nabla \cdot (\rho_i \boldsymbol{u}_i) = 0, \tag{1}$$

$$\rho_i \left(\frac{\partial \boldsymbol{u}_i}{\partial t} + \boldsymbol{u}_i \cdot \nabla \boldsymbol{u}_i \right) = -\nabla \cdot \boldsymbol{t}_i + n_i \boldsymbol{F}_i + \boldsymbol{\phi}_i, \tag{2}$$

where ρ_i, the mass density, is the product of the particle mass m_i and number density n_i (note that $\rho_i = \rho_{pi} v_i = m_i n_i$ where ρ_{pi} is the material density of the particle and v_i is the volume fraction); $\boldsymbol{u}_i$ is the mean velocity; $\boldsymbol{t}_i$ is the stress tensor; $\boldsymbol{F}_i$ is the external force; and $\boldsymbol{\phi}_i$ is the momentum source due to collisions between unlike particles. (The above set is often written in an equivalent form, in which a mixture momentum balance is obtained by adding together N species balances, and $N-1$ diffusion velocity balances for species i are obtained via algebraic manipulations of the species momentum balances. See Jenkins & Mancini (1987) for details.) To obtain the required constitutive relations for $\boldsymbol{t}_i$ and $\boldsymbol{\phi}_i$, methods from the dense-gas kinetic theory are employed (see, for example, Chapman & Cowling 1970). The resulting expressions are found to depend on the species granular temperature $T_i = m_i \langle C_i^2 \rangle / 3$, where $\langle C_i^2 \rangle$ represents the average of the squared peculiar (fluctuation relative to mass-average) velocity. Accordingly, the solution of a granular energy balance for each species is also required. (This set of equations can also be written in a mixture form, where the mixture temperature T for a binary mixture is defined as $T = (n_1 T_1 + n_2 T_2)/n$.)

For rapidly flowing granular mixtures, numerous kinetic-theory models applicable to general flow fields have been reported in the literature (Jenkins & Mancini 1987, 1989; Zamankhan 1995; Arnarson & Willits 1998; Willits & Arnarson 1999; Huilin, Gidaspow & Manger 2001; Garzó & Dufty 2002; Rahaman, Naser & Witt 2003). Generally speaking, two different approaches have been used in the development of such theories. The first approach is based on an assumed form of the velocity distribution function, whereas the second approach is based on a systematic expansion about a zeroth-order solution to the conservation equation (e.g. via Chapman–Enskog or Grad expansion). The latter approach does not involve an assumed form of the distribution function. For mixtures, only the theory of Garzó & Dufty (2002) is based on a systematic expansion about the solution. The starting point of their theory is the Boltzmann equation, which restricts the application of the theory to dilute flows. On the other hand, those theories based on an assumed form of the distribution function (Jenkins & Mancini 1987, 1989; Zamankhan 1995; Arnarson & Willits 1998; Willits & Arnarson 1999; Huilin *et al.* 2001; Rahaman *et al.* 2003) have been derived from the Enskog equation, and thus can be applied to moderately dense systems as well. Since the scope of the current work includes moderately dense systems, the ensuing discussion is restricted to such theories.

Reference	Single-particle velocity distribution	Energy distribution	Radial distribution function	System dimension
Jenkins & Mancini (1987)	Maxwellian	Non-equipartition	SET	2 and 3
Jenkins & Mancini (1989)	Non-Maxwellian	Equipartition	RET	3
Zamankhan (1995)	Non-Maxwellian	Equipartition	RET	3
Arnarson & Willits (1998)	Non-Maxwellian	Equipartition	RET	3
Willits & Arnarson (1999)	Non-Maxwellian	Equipartition	RET	2
Huilin *et al.* (2001)	Maxwellian	Non-equipartition	SET	3
Rahaman *et al.* (2003)	Maxwellian	Non-equipartition	SET	3

TABLE 1. Overview of kinetic theory models for granular mixtures in a general flow field. (All models are for binary mixtures except Zamankhan (1995).)

The differences between kinetic theories of mixtures (based on an assumed form of the distribution function) can be traced to corresponding assumptions used in the derivation process, as given in table 1. Specifically, the three basic differences are (i) Maxwellian *vs.* non-Maxwellian single-particle velocity distribution, (ii) equipartition *vs.* non-equipartition of energy between unlike particles, and (iii) standard Enskog (SET) theory *vs.* revised Enskog theory (RET) treatment of radial distribution function at contact. The first two simplifying assumptions, namely a Maxwellian velocity distribution and an equipartition of energy, are strictly true only for perfectly elastic spheres in a uniform steady state (Chapman & Cowling 1970). Furthermore, the Maxwellian assumption precludes any kinetic contribution to the shear stress (Campbell 1990), thereby limiting the corresponding theory to collision-dominated (or moderately dense) flows. With regard to the second difference, because the equipartition assumption provides an explicit relation between the species temperatures ($T_1 = T_2 = \cdots = T_N$), invoking it leads to a single-temperature theory in the mixture temperature $T(= T_1 = T_2 = \cdots)$, as compared to the multi-temperature theory (i.e. a separate equation for each T_i) required for systems without an equipartition of energy. The third difference between existing theories concerns the point (along the line of centres between particles) at which the radial distribution function is evaluated. Unlike SET, the RET proposed by van Beijeren & Ernst (1973) is found to be consistent with irreversible thermodynamics.

Based on the above discussion, the most complete theory for the rapid flow of granular mixtures is one which employs RET and accounts for both a non-Maxwellian distribution and a non-equipartition of energy. None of the existing theories falls under this category (table 1), as incorporating all of these items adds non-trivial complexity to the derivation and the final form of the constitutive relations. (Garzó & Dufty (2002) developed a kinetic theory for a binary mixture which inherently allows for both non-Maxwellian and non-equipartition effects. As mentioned above, however, their theory is limited to dilute systems, whereas the scope of the current discussion includes moderately dense systems.) Nevertheless, if the ultimate goal is to establish a theory which gives predictions of reasonable accuracy without unnecessary complexity, such a complete theory may or may not be necessary. To make such a determination, the influence of these common assumptions on the predictive ability of kinetic-theory models must be ascertained.

Several previous investigations provide insight into the impact of typical kinetic-theory assumptions. Concerning the treatment of the single-particle velocity distribution, a number of experimental, simulation and theoretical studies of monodisperse

systems have indicated that a Maxwellian distribution is not strictly upheld (e.g. Campbell 1990; Goldshtein & Shapiro 1995; Goldhirsch & Tan 1996; Esipov & Pöschel 1997; van Noije & Ernst 1998; Brey, Cubero & Ruiz-Montero 1999; Losert *et al.* 1999; Kudrolli & Henry 2000). A gauge of the importance of this effect on kinetic-theory predictions is given by Willits & Arnarson (1999). In particular, a comparison of shear viscosities is given between the binary kinetic theories of Willits & Arnarson (1999) and Jenkins & Mancini (1987) and simulations of perfectly elastic disks with a diameter ratio of 1.25. Because the Jenkins & Mancini (1987) theory is first simplified via an equipartition-of-energy assumption (which is valid for elastic disks), the sole difference between the predictions is that the Jenkins & Mancini (1987) theory is based on an assumption of a Maxwellian velocity distribution, and the Willits & Arnarson (1999) theory accounts for a non-Maxwellian distribution. (See table 1. Also, the mixture momentum flux is the same for SET and RET (van Beijeren & Ernst 1973), and thus is not a source of differences in this comparison.) Over a range of overall solids fractions from 0.05 to 0.4, the Willits & Arnarson (1999) theory displays very good agreement with simulation values. The Jenkins & Mancini (1987) predictions are significantly lower in value, however, since the Maxwellian assumption precludes the kinetic contribution to the shear stress and simplifies the collisional contribution to the stress. Hence, these results indicate that a non-Maxwellian velocity distribution is critical for accurate predictions of the shear stress. With regard to the treatment of the energy distribution, a wide range of experimental (Feitosa & Menon 2002; Wildman & Parker 2002), simulation (Clelland & Hrenya 2002; Dahl, Clelland & Hrenya 2002; Alam & Luding 2003; Paolotti *et al.* 2003), and theoretical (Garzó & Dufty 1999; Barrat & Trizac 2002; Montanero & Garzó 2003) studies provide evidence that an equipartition of energy does not exist, particularly for highly dissipative (inelastic) systems in which the mass ratio of unlike particles is not near unity. Nonetheless, a comparison (Clelland & Hrenya 2002) between Willits & Arnarson (1999) theory, which does not account for a non-equipartition, and molecular-dynamics (MD) simulations of inelastic particles show good agreement. In particular, over a wide range of solids concentrations and diameter ratios, the shear and normal components of the stress tensor are well predicted by the theory, despite temperature ratios as high as 8 observed in the simulations. Such results may indicate that equipartition effects have a small effect on kinetic-theory predictions, though the observed agreement may also be fortuitous.

Collectively, these previous investigations indicate that a non-Maxwellian distribution is necessary for reliable kinetic-theory predictions, whereas the need to account for a non-equipartition of energy is less clear. The first part of the current work is targeted at gaining a better understanding of the latter effects. In particular, the Jenkins & Mancini (1987) theory is employed both with and without the equipartition assumption to a simple shear-flow system, and comparisons are made to both MD simulations and the Arnarson & Willits (1998) theory. (Although predictions from the Jenkins & Mancini (1987) theory have appeared in the literature, all previous applications of the theory have incorporated the equipartition assumption.) The current results indicate that the temperature ratio between unlike particles is well-predicted by the non-equipartition theory of Jenkins & Mancini (1987). The corresponding stress predictions, however, are only slightly better than those obtained when an equipartition assumption is imposed, both of which are inferior to the non-Maxwellian predictions of Arnarson & Willits (1998). Although these results appear to indicate that a non-equipartition treatment adds unwarranted complexity to the model, an analysis of a more complex flow field, which is undertaken as the second part of this

effort, suggests otherwise. In particular, an examination of the governing equations for a segregating system reveals that a non-equipartition of energy gives rise to additional driving forces associated with size/density segregation. (Note that the simple shear system included in the first part of the investigation does not display size segregation owing to a zero temperature gradient.) The new driving forces involve gradients in species temperature, whereas theories based on the equipartition assumption depend only on gradients in mixture temperature. To assess the importance of this new driving force, the results from MD simulations of binary mixtures in a segregating flow field are compared to Jenkins & Mancini (1987) theory. The segregating system is characterized by zero mean flow between two impenetrable boundaries of constant, but unequal, granular temperatures. Results indicate that one of the non-equipartition driving forces is of similar magnitude to the largest of equipartition driving forces for systems with moderate values of mass differences and restitution coefficients. Furthermore, unlike previous observations of non-equipartition, the more massive species exhibits a smaller species temperature than the lighter species over small regions of the domain. A physical rationale for this behaviour is presented.

2. Non-segregating flow system: simple shear flow

In the first portion of this work, an unbounded simple shear flow is considered. Owing to the uniform velocity gradient, the granular temperatures and stress components are constant throughout the domain. Also, owing to the uniformity of the flow domain, particle segregation does not occur. (Transient inhomogeneities in particle concentration, or clusters, were observed in the MD simulations, as has been documented by several workers for simple shear flows of identical particles (e.g. Hopkins & Louge, 1991; Tan & Goldhirsch 1997). The time-averaged concentration of particles, however, did not vary across the simulation domain.)

2.1. *Computational approach*

Three-dimensional molecular-dynamics simulations are employed for binary mixtures of frictionless spherical particles engaging in instantaneous collisions. (These assumptions are identical to those of the kinetic-theory models.) For a detailed description of the computational algorithm, see Dahl *et al.* (2002).

The input parameters for each simulation include L_x, L_y and L_z, the length of the simulation domain in the x, y and z directions; d_1, the diameter of type 1 particles; m_1, the mass of a type 1 particle; d_1/d_2, the ratio of the diameters of the particle types; ν_1/ν_2, the ratio of the solid-volume fractions of the particle types; ρ_{p1}/ρ_{p2}, the ratio of the material densities of the particle types; ν, the total solids-volume fraction; $\mathrm{d}u_x/\mathrm{d}y$, the shear rate (where $\boldsymbol{u}$ is the mass-average velocity of the mixture); and e, the coefficient of restitution for all particle interactions. For all simulations, the domain lengths are set equivalently ($L_x = L_y = L_z$) so that the simulation domain is cubic and the characteristic dimension is hereby referred to as L.

The dimensionless parameters that describe the system include d_1/d_2, with values examined between 1 and 4; ρ_{p1}/ρ_{p2}, with values between 0.1 and 5; ν_1/ν_2, with values between 0.5 and 4; ν, with values of 0.1, 0.3 or 0.5; e, with values of either 0.8 or 0.95; and L/d_1, with values of either 8.9 or 4.45 (the latter value used for $\nu = 0.5$, and the special case $\nu = 0.3$, $\nu_1/\nu_2 = 0.5$). The value of L/d_1 was chosen so that the stresses would not be sensitive to perturbations in L/d_1 (for details, see Dahl *et al.* 2002). All other parameters, namely $\mathrm{d}u_x/\mathrm{d}y$, L, and m_1 were set equal to 1 for convenience.

The outputs from the simulations include the stresses and granular temperatures. The collection of stress components is described by Dahl *et al.* (2002). The mixture granular temperature, is defined as

$$T = \frac{\sum_{j=1}^{N} \frac{1}{3} m_j C_j^2}{N}, \tag{3}$$

where C_j is the magnitude of the fluctuating particle velocity relative to the mass-averaged velocity. The mean granular temperature is obtained by averaging 100 000 instantaneous measurements. Both the mixture granular temperature (T) and the granular temperature for each species (T_1 and T_2) are measured. Prior to reporting, all stresses are made dimensionless via division by $\rho_{p1} d_1^2 (\mathrm{d}u_x/\mathrm{d}y)^2$ and the granular temperature is non-dimensionalized using the quantity $\rho_{p1} d_1^5 (\mathrm{d}u_x/\mathrm{d}y)^2$.

2.2. *Results and discussion*

The kinetic-theory predictions of Jenkins & Mancini (1987), applied both with and without the equipartition assumption, and of Arnarson & Willits (1998) were compared with molecular-dynamics simulations to assess the influence of various assumptions. For simple shear, the system of governing equations obtained from theory reduces to the granular energy balance(s), in which production due to shear is balanced by dissipation due to inelastic collisions. For the case of the full Jenkins & Mancini theory (i.e. including non-equipartition effects), the detailed form of the governing equations is contained in table 2. For each of the theories, analytical solutions for the granular temperature(s) were obtained, which were then used to evaluate the corresponding stress components. Over the wide parameter space examined, the trends were found to be similar. As expected, the predictive ability of the Jenkins & Mancini (1987) theory worsens considerably for lower overall solids fractions ($\sim$0.1) since the Maxwellian assumption precludes any kinetic contribution to the shear stress. Hence, in order to compare the assumptions contained in the various theories better, attention is paid to the parameter range in which predictions are expected to be most valid. More specifically, only a few representative cases at larger volume fractions (in which collisional contributions are important) are explicitly discussed below.

Figure 1 provides a comparison of the non-dimensional normal (figure 1*a*) and shear (figure 1*b*) stress components as determined from molecular dynamics and both kinetic theories for d_1/d_2 in the range of 1–4 ($m_1/m_2 = 1$–64). For this figure, $\rho_{p1}/\rho_{p2} = 1$, $\nu = 0.3$, $\nu_1/\nu_2 = 0.5$, $e = 0.95$ and $L/d_1 = 4.45$. In this and subsequent diagrams, individual points represent the MD results and lines indicate kinetic theory predictions. Although simulation results are shown for each of the normal components (t_{xx}, t_{yy} and t_{zz}), the theoretical predictions are denoted by a single line since the theories are based on the assumption $t_{xx} = t_{yy} = t_{zz}$.

An inspection of figure 1 reveals that the predictions of both theories capture the qualitative nature of the simulation results. Namely, as the diameter ratio increases, the normal and shear stress of both simulation and theory decrease. The stress predictions of the Arnarson & Willits theory are slightly higher than the MD simulation results, but in better agreement than the stress predictions of the Jenkins & Mancini theory (with or without an assumption of equipartition of energy), which are considerably lower than MD simulation results. For example, the shear stress predictions of the Arnarson & Willits theory overpredict the results of MD simulations by 20 % at $d_1/d_2 = 4.0$ and by 8.8 % at $d_1/d_2 = 1.0$. In contrast, the shear stress predictions of the Jenkins & Mancini theory with equipartition of energy underpredict the results

Granular energy balance: species 1

$$t_{xy,1}\frac{\mathrm{d}u_x}{\mathrm{d}y} = \gamma_1$$

Granular energy balance: species 2

$$t_{xy,2}\frac{\mathrm{d}u_x}{\mathrm{d}y} = \gamma_2$$

Relation arising from definitions

$$T \equiv \frac{1}{n_1+n_2}(n_1T_1+n_2T_2) \quad \text{and} \quad T_i \equiv T+\theta_i\text{:}$$
$$n_1\theta_1+n_2\theta_2 = 0$$

Constitutive relations

$$t_{xy,i} = \sum_{k=A,B} t_{xy,ik} = \sum_{k=A,B} -\frac{2\pi}{15}(1+e)g_{ik}r_{ik}^4 n_i n_k \left(\frac{2m_im_k}{\pi m_{ik}}\right)^{1/2}\left(\frac{\mathrm{d}u_x}{\mathrm{d}y}\right)T^{1/2}$$

$$\gamma_i = 2(1+e)g_{ik}r_{ik}^2 n_i n_k T^{1/2}\left\{2\left(\frac{2\pi m_im_k}{m_{ik}}\right)^{1/2}\left(\frac{\theta_i-\theta_k}{m_{ik}}\right)\right.$$
$$\left. -\frac{m_k}{m_{ik}}(1-e)\left(\frac{2\pi m_{ik}}{m_im_k}\right)^{1/2}\left[T+\frac{3}{2}\left(\frac{m_i\theta_k+m_k\theta_i}{m_{ik}}\right)\right]\right\}$$

Additional definitions

$$g_{ik} = \frac{1}{1-v}+\frac{6r_ir_k}{(r_i+r_k)}\frac{\xi}{(1-v)^2}+8\left(\frac{r_ir_k}{r_i+r_k}\right)^2\frac{\xi^2}{(1-v)^3}$$
$$v = \tfrac{4}{3}\pi\left(n_1r_1^3+n_2r_2^3\right)$$
$$\xi = \tfrac{2}{3}\pi\left(n_1r_1^2+n_2r_2^2\right)$$
$$m_{ik} = m_i+m_k$$
$$r_{ik} = r_i+r_k$$

TABLE 2. Governing equations for simple shear flow based on kinetic theory of Jenkins & Mancini (1987). For cases in which the equipartition assumption is imposed, $\theta_1 = \theta_2 = 0$.

of MD simulations by 51 % at $d_1/d_2 = 4.0$ and 59 % at $d_1/d_2 = 1.0$. Analogous results are obtained for cases in which ρ_{p1}/ρ_{p2} is varied instead of d_1/d_2 (not shown for the sake of brevity). Similar trends are also observed for the other solids fractions and solids fraction ratios investigated, with few exceptions. (Specifically, at high solids fractions and solid fraction ratios, the shear stress predictions of the Jenkins & Mancini theory, without equipartition, become greater than those of the Arnarson & Willits theory (figure not shown). This 'crossover' is more evident at lower coefficient of restitutions ($e = 0.80$). Despite the presence of a crossover, the stress predictions of the Arnarson & Willits theory still outperform those of the Jenkins & Mancini theory.) These observations indicate that a non-Maxwellian velocity distribution is critical for reliable stress predictions (as is consistent with Willits & Arnarson 1999).

One point of interest is that the stress predictions of the Jenkins & Mancini theory with the assumption of equipartition of energy differ very little from the stress predictions without the assumption of equipartition of energy. Specifically, in figure 1(*b*), the shear stress predictions of the Jenkins & Mancini theory with versus without the equipartition assumption differ by a maximum of 3.4 % at the largest diameter ratio investigated. At a limiting diameter ratio of 1.0 (monodisperse), no deviation exists between the stress predictions obtained with or without an equipartition of energy. The difference between the stress predictions (with versus without an equipartition

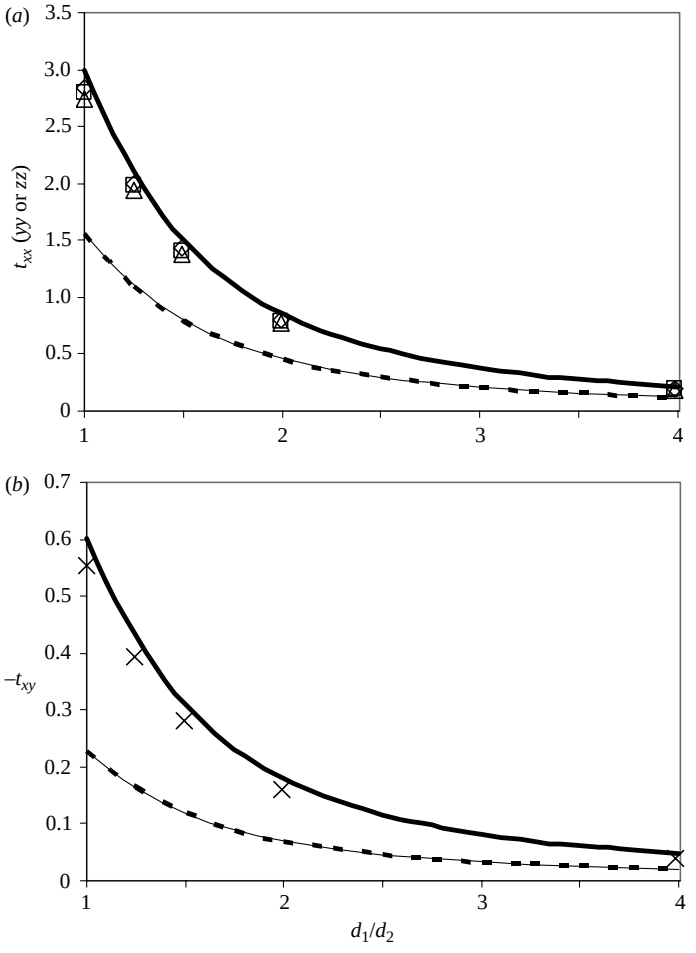

FIGURE 1. Non-dimensional (*a*) normal and (*b*) shear stress components of a binary mixture of smooth hard spheres engaged in simple shear flow. MD simulations (points) with t_{xx} (squares), t_{yy} (diamonds) and t_{zz} (triangles); Arnarson & Willits (1998) predictions (thick solid line); Jenkins & Mancini (1987) predictions with equipartition (dashed line) and without equipartition (thin solid line). Relevant parameters: $\rho_{p1}/\rho_{p2} = 1.0$, $e = 0.95$, $L/d_1 = 4.45$, $\nu = 0.3$, $\nu_1/\nu_2 = 0.5$.

assumption) is more pronounced at lower coefficients of restitution (figure not shown) and higher diameter ratios.

Despite the essentially negligible impact of a non-equipartition treatment on stress predictions, a significant non-equipartition of energy is present. To demonstrate the degree of non-equipartition, figure 2 displays the granular temperature ratio (T_1/T_2) at two coefficients of restitution ($e = 0.95$ and $e = 0.80$) versus d_1/d_2 for three different solid volume fractions $\nu_1/\nu_2 = 4.0$ (figure 2*a*), $\nu_1/\nu_2 = 1.0$ (figure 2*b*), and $\nu_1/\nu_2 = 0.5$ (figure 2*c*). In figure 2, $\rho_{p1}/\rho_{p2} = 1$ and $\nu = 0.3$ with $L/d_1 = 8.9$ in subplots (*a*) and (*b*) and $L/d_1 = 4.45$ in subplot (*c*). (Although the diameter ratio is used as the abscissa, the mass ratio could also be used, and in this case, an increasing diameter ratio also implies an increasing mass ratio.) Evident in these diagrams is the disparity of granular energy between the two species. The Jenkins & Mancini theory without the equipartition-of-energy assumption is able to predict the non-equipartition in a

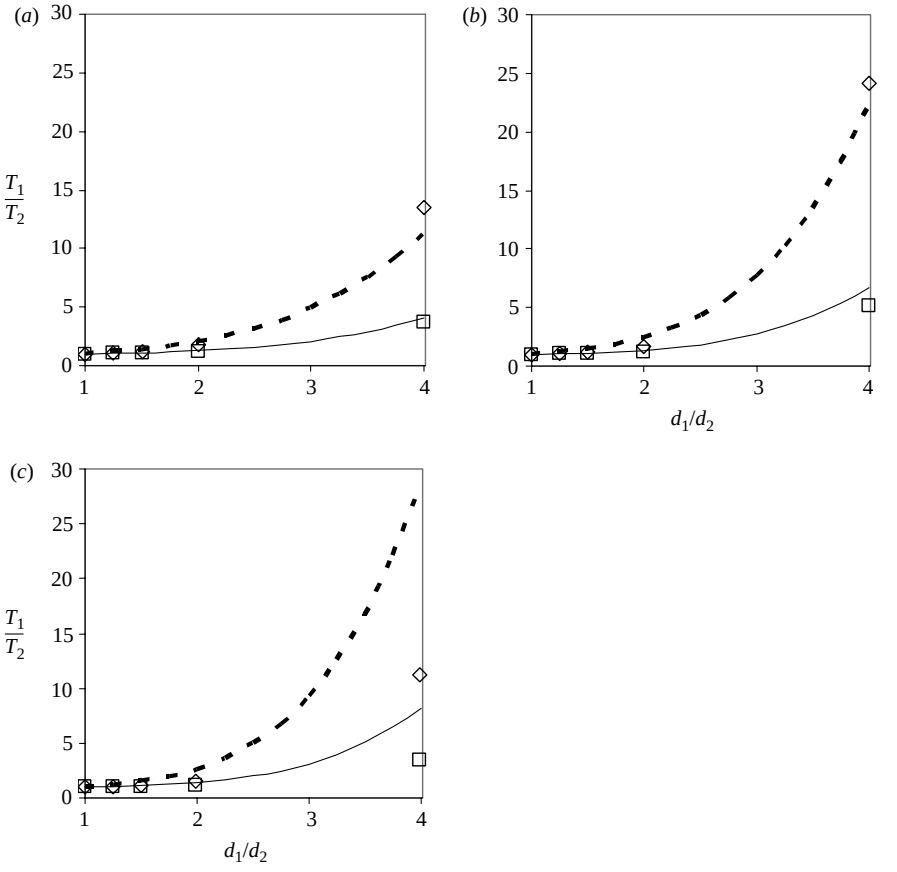

FIGURE 2. Granular temperature ratio of species 1 to species 2 (T_1/T_2) at two coefficients of restitution for (*a*) $\nu_1/\nu_2 = 4.0$, (*b*) $\nu_1/\nu_2 = 1.0$ (*c*) $\nu_1/\nu_2 = 0.5$. MD simulations for $e = 0.95$ (squares) and $e = 0.8$ (diamonds); Jenkins and Mancini (1987) predictions without equipartition for $e = 0.95$ (solid line) and $e = 0.8$ (dashed line). Relevant parameters: $\rho_{p1}/\rho_{p2} = 1.0$, $L/d_1 = 4.45$, $\nu = 0.3$.

qualitatively correct manner. Namely, the predicted granular temperature of species 1 is greater than that of species 2, and the difference in temperatures increases with increasing diameter ratio (or mass ratio) and decreasing restitution coefficient. For example, in figure 2(*a*), $T_1/T_2 = 3.7$ at $e = 0.95$ and $T_1/T_2 = 13.5$ at $e = 0.8$, both at $d_1/d_2 = 4.0$ ($m_1/m_2 = 64$). This trend is captured well by the Jenkins & Mancini theory. From a quantitative standpoint, for a given overall solids fraction (ν), the predictions of the Jenkins & Mancini theory are in very good agreement with MD simulation at higher solids fraction ratio ν_1/ν_2 (figure 2*a*). As ν_1/ν_2 decreases, the level of accuracy is seen to decrease (figures 2*a*–2*c*). For example, at $d_1/d_2 = 2.0$ ($m_1/m_2 = 8$) with $e = 0.8$, the predictions from the Jenkins & Mancini theory differ from MD simulations by only 14 % at $\nu_1/\nu_2 = 4.0$, and by 72 % at $\nu_1/\nu_2 = 0.5$. Overall, the non-equipartition treatment of Jenkins & Mancini is in fairly good agreement with MD simulations.

To summarize, a non-Maxwellian velocity distribution has been shown to be important for accurate stress predictions (as was demonstrated by Willits & Arnarson 1999), whereas accounting for non-equipartition effects has relatively little impact. Nonetheless, an equipartition of energy is not upheld away from the equal-mass

($m_1/m_2 = 1.0$) and elastic ($e = 1.0$) limits, as is predicted well by the non-equipartition treatment of Jenkins & Mancini. In the following section, the impact of a non-equipartition of energy is explored in the context of a more complex flow system.

3. Segregating flow system

For systems which are not characterized by a constant granular temperature across the flow domain (unlike the simple shear-flow system), a segregation of particles according to size and/or density may occur. The driving forces for such segregation have been explored by previous investigators (and are outlined by Jenkins 1998). All of these previous works, however, are based on kinetic-theory models in which an equipartition of energy is assumed. In particular, Hsiau & Hunt (1996) used the later Jenkins & Mancini theory (1989) to investigate the driving forces for segregation. An examination of the equation governing segregation, namely the balance for the diffusion velocity, revealed the following driving forces: external forces, pressure gradient, species concentration gradient and granular temperature gradient. (Because granular pressure is a function of both the species concentration and granular temperature, the diffusion velocity equation can be expressed as a balance between external forces and gradients in concentration and temperature only.) Furthermore, a theoretical analysis of an oscillatory no-flow system and a sheared system indicated that large or heavier particles tend to segregate toward regions of lower T. More recently, Arnarson & Jenkins (2000) also analysed the diffusion velocity equation to explore how RET and SET lead to different theories for segregation. They found that the different theories lead to different coefficients for the species gradients, but do not impact the coefficients of the pressure or temperature gradients. To assess the ability of kinetic theories to predict size and density segregation in binary mixtures, several workers have compared theoretical predictions with simulation data. Because the systems investigated involve relatively small differences in particle masses, the equipartition assumption is not significantly violated. For example, Louge *et al.* (2001) examined the segregation of two binary systems in a microgravity shear cell. The first system contained particles with $d_1/d_2 \sim 1.25$, $\rho_{p1}/\rho_{p2} = 0.32$ and $e = 0.93$ and the second system was represented by $d_1/d_2 \sim 1.24$, $\rho_{p1}/\rho_{p2} = 1$ and $e = 0.93$. The predictions obtained using a simplified kinetic theory targeted at particles with small differences in masses and radii of the two species, compared well with molecular-dynamics simulations, particularly for lower values of the overall solids volume fraction. For the case of gravity-driven chute flow, Khakhar, McCarthy & Ottino (1999) compared model predictions based on the Jenkins & Mancini (1989) theory with discrete-particle simulations. Using temperature profiles obtained from the simulation as input to the diffusion equation (instead of solving for temperature field from kinetic theory), the agreement for equal-sized particles with $\rho_{p1}/\rho_{p2} = 2$ and $e = 0.9$ was found to be good except near the boundary region. Similar observations were made for a system of equal-density particles with $d_1/d_2 \sim 1.4$ and $e = 0.9$.

As mentioned above, these previous investigations on segregation are all based on an equipartition assumption. To determine the effects of a non-equipartition of energy on the segregation phenomenon, the diffusion velocity equation, along with constitutive relations accounting for a non-equipartition, is examined. For simplicity, a three-dimensional binary system composed of species 1 and 2 is considered (though the analysis is applicable to systems of arbitrary dimensions and number of species). For such a system, the diffusion velocity equation is obtained by dividing each of the species momentum balances, equation (2), by their respective mass densities (ρ_i), and

then subtracting species balance 2 from that of 1:

$$\frac{\partial}{\partial t}(\boldsymbol{v}_1-\boldsymbol{v}_2)+(\boldsymbol{u}_1\cdot\nabla)\boldsymbol{v}_1-(\boldsymbol{u}_2\cdot\nabla)\boldsymbol{v}_2+(\boldsymbol{v}_1\cdot\nabla)\boldsymbol{u}-(\boldsymbol{v}_2\cdot\nabla)\boldsymbol{u}$$
$$=-\frac{1}{\rho_1}\nabla\cdot\boldsymbol{t}_1+\frac{1}{\rho_2}\nabla\cdot\boldsymbol{t}_2+\frac{1}{m_1}\boldsymbol{F}_1-\frac{1}{m_2}\boldsymbol{F}_2+\frac{1}{\rho_1}\phi_1-\frac{1}{\rho_2}\phi_2. \quad (4)$$

In this equation, $\boldsymbol{v}_i$ is the diffusion velocity, defined as $\boldsymbol{v}_i=\boldsymbol{u}_i-\boldsymbol{u}$, where $\boldsymbol{u}=\Sigma\rho_i\boldsymbol{u}_i/\Sigma\rho_i$ is the mass-averaged mixture velocity. (Note that for simple shear flow, this equation is solved identically; hence, modifications to this equation do not impact the corresponding stress predictions). Invoking the common assumption that the inertia associated with diffusion and the nonlinear terms $(\boldsymbol{v}_i\cdot\nabla)\boldsymbol{u}$ are negligible, the above equation is simplified to

$$0=-\frac{1}{\rho_1}\nabla\cdot\boldsymbol{t}_1+\frac{1}{\rho_2}\nabla\cdot\boldsymbol{t}_2+\frac{1}{m_1}\boldsymbol{F}_1-\frac{1}{m_2}\boldsymbol{F}_2+\frac{1}{\rho_1}\boldsymbol{\phi}_1-\frac{1}{\rho_2}\boldsymbol{\phi}_2. \quad (5)$$

This form of the diffusion equation, which is identical to that used by the previous investigators to analyse the segregation phenomenon (see, for example, Jenkins 1998; Arnarson & Jenkins 2000), is now explored in the context of a non-equipartition of energy. Specifically, the constitutive relations for $\boldsymbol{t}_i$ and $\boldsymbol{\phi}_i$ developed by Jenkins & Mancini (1987) are considered. (Although the study by Jenkins & Mancini (1987) does include a derivation of the diffusion equation, the analysis contained therein is restricted to a simplified case in which the equipartition of energy is upheld.) The quantity $\boldsymbol{\phi}_i$ is found by Jenkins & Mancini (1987) to depend only on the mixture temperature T and not on the species temperature T_i, whereas the stress tensor $\boldsymbol{t}_i$ is found to depend on both quantities:

$$\boldsymbol{\phi}_i=K_{ik}T\left[\left(\frac{m_k-m_i}{m_i+m_k}\right)\nabla\ln T+\nabla\ln\frac{n_i}{n_k}+\frac{4}{r_i+r_k}\left(\frac{2m_im_k}{\pi(m_i+m_k)T}\right)^{1/2}(\boldsymbol{v}_k-\boldsymbol{v}_i)\right] \quad \text{for } i\neq k, \quad (6)$$

$$\boldsymbol{t}_i=n_i(T+\theta_i)\boldsymbol{I}+\sum_{k=1,2}K_{ik}\left(T+\frac{m_i\theta_k+m_k\theta_i}{m_i+m_k}\right)\boldsymbol{I}, \quad (7)$$

where r_i refers to the radius of particle i; K_{ik} are functions of the number density, particle diameter, and restitution coefficient (as detailed in table 3); and $\theta_i=T_i-T$ represents the deviation of the species temperature from the mixture temperature ($\theta_i=0$ when equipartition is assumed). In determining (7), the diffusive and viscous contributions to the stress tensor $\boldsymbol{t}_i$ are assumed negligible, as was done in the previous analyses (e.g. Jenkins & Mancini 1987; Jenkins 1998). To more clearly illustrate those terms associated with non-equipartition effects, the above equation can be rewritten as

$$\boldsymbol{t}_i=P_i\boldsymbol{I}+P_{new,i}\boldsymbol{I}, \quad (8)$$

where

$$P_i=\left(n_i+\sum_{k=1,2}K_{ik}\right)T \quad (9)$$

is the species partial pressure obtained when an equipartition of energy is assumed, and

$$P_{new,i}=n_i\theta_i+\sum_{k=1,2}K_{ik}\left(\frac{m_i\theta_k+m_k\theta_i}{m_i+m_k}\right) \quad (10)$$

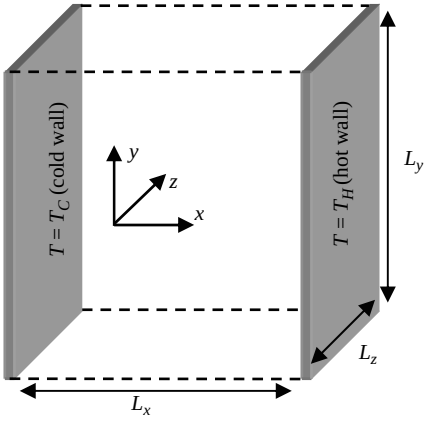

FIGURE 3. Segregating flow system.

represents the non-equipartition contribution to the species partial pressure. Recognizing that $\boldsymbol{\phi}_1 = -\boldsymbol{\phi}_2$ and substituting (6) and (8)–(10) into (5) leads to

$$\boldsymbol{v}_1 - \boldsymbol{v}_2 = -\frac{n^2}{n_1 n_2} D_{12} \boldsymbol{d}_1, \tag{11}$$

where $n = n_1 + n_2$, and the coefficient of ordinary diffusion D_{12} and the diffusion force $\boldsymbol{d}_1$ are defined as

$$D_{12} = \frac{n_1 n_2}{n} \frac{r_1 + r_2}{K_{12}} \left(\frac{\pi}{32} \frac{m_1 + m_2}{m_1 m_2} T \right)^{1/2}, \tag{12}$$

$$\boldsymbol{d}_1 = \frac{1}{\rho n T} [\rho_2 \nabla P_1 - \rho_1 \nabla P_2] + \frac{1}{\rho n T} [\rho_2 \nabla P_{new,1} - \rho_1 \nabla P_{new,2}] - \frac{\rho_1 \rho_2}{\rho n T} \left[\frac{\boldsymbol{F}_1}{m_1} - \frac{\boldsymbol{F}_2}{m_2} \right] - \frac{K_{12}}{n T} \left(\frac{m_2 - m_1}{m_1 + m_2} \right) \nabla T - \frac{K_{12}}{n} \left[\frac{1}{n_1} \nabla n_1 - \frac{1}{n_2} \nabla n_2 \right], \tag{13}$$

where $\rho = \rho_1 + \rho_2$. Equations (11)–(13) illustrate the driving forces associated with size and density segregation. Namely, when an equipartition-of-energy assumption is made (i.e. $P_{new,1} = P_{new,2} = 0$), the second bracketed term on the right-hand side of (13) vanishes. Correspondingly, the diffusion force is composed of driving forces associated with ∇n_1, ∇n_2 and ∇T (recall P_1 and P_2 are functions of n_1, n_2 and T only; see (9)). However, when the equipartition assumption is lifted, additional driving forces associated with $\nabla \theta_1$ and $\nabla \theta_2$ arise from the $P_{new,1}$ and $P_{new,2}$ terms present in (13). Additional terms associated with the ∇n_1 and ∇n_2 driving forces also arise since $P_{new,1}$and $P_{new,2}$ are also functions of n_1 and n_2. The presence of such driving forces has not been recognized in previous investigations on size and density segregation.

3.1. *Computational approach*

As in the simple shear flow study, this work employs three-dimensional hard-sphere simulations of binary granular mixtures and treats the particles as frictionless inelastic spheres engaging in instantaneous collisions. Unlike the simple shear flow simulation, however, the segregating system is characterized by a granular temperature gradient, which causes both bulk (overall) segregation and segregation of particles according to size and/or density (species segregation). As portrayed in figure 3, the simulation box is bounded on the left and right by motionless walls of constant, but unequal,

granular temperatures. The four remaining sides of the simulation domain, namely the upper and lower and the forward and backward boundaries, are standard periodic conditions. No body forces are present, and hence the system is characterized by zero mean flow.

As previously mentioned, the simulation is bounded in the x-direction by walls of set temperature (T_{set}). Particles colliding with a constant-temperature wall are given a post-collision velocity that is consistent with T_{set} of the given wall. Specifically, the post-collision speed is determined using the Box Muller method for generating Gaussian distributions (Press *et al.* 1992):

$$c_1 = \sqrt{-\frac{4T_{set}}{3m_i}\ln(z_1)}\,\cos(2\pi z_2), \tag{14}$$

$$c_2 = \sqrt{-\frac{4T_{set}}{3m_i}\ln(z_3)}\,\cos(2\pi z_4), \tag{15}$$

$$c_3 = \sqrt{-\frac{4T_{set}}{3m_i}\ln(z_5)}\,\cos(2\pi z_6), \tag{16}$$

and

$$c_{post} = \sqrt{c_1^2 + c_2^2 + c_3^2}, \tag{17}$$

where $z_1 - z_6$ are random numbers uniformly distributed in the interval [0, 1] and c_{post} is the post-collision speed of the particle. The post-collision trajectory of the particle is determined based on the pre-collision trajectory of the particle. In particular, the sign (+ or −) of the pre-collision component of particle velocity normal to the wall is reversed after collision. The sign of the pre-collision components of particle velocity parallel to the wall (in the y and z directions) may be unchanged or reversed during a collision, determined by random multiplication with -1 or 1. This random adjustment of the components of particle velocity in the directions parallel to the constant-temperature wall is performed in order to avoid the appearance of persistent net motion of particles (Luding, Strauss & McNamara 2000).

To help ensure that simulation results are not sensitive to the detailed form of the boundary conditions, other schemes giving rise to constant-temperature walls were also investigated. As an alternative, the post-collisional components of particle velocity parallel to the wall (in the y and z directions) are determined directly by (14) and (15), while the post-collisional component of particle velocity normal to the wall is given by

$$c_{post,x} = \sqrt{-\frac{4T_{set}}{3m_i}\ln(z_5)} \tag{18}$$

and the sign of this component is reversed after collision. The results arising from both methods are nearly identical. In both of the aforementioned schemes, an equipartition of energy is imposed at the walls. The effect of enforcing a non-equipartition at the walls was also tested. This boundary condition only slightly alters the species temperature in the near-wall region, and does not impact the flow profiles in the domain interior. Hence, the simulations described here are based on the boundary conditions described by (14)–(17).

Like the simple shear system, the particles are initially placed on a nearly cubic lattice. Small random displacements move particles from their node positions, and any existing overlaps are removed by making further random displacements in their position. Unlike the simple shear system, temperature is not uniform throughout the

domain and a granular temperature gradient does exist. As an initial estimate, particles are assigned velocities from a Maxwellian distribution, consistent with their position along an assumed linear temperature profile between the walls of set temperature. The actual temperature profile that develops is not linear, but the linear assumption provides a basis for the initial condition.

In this simulation, a time-stepped algorithm is used (as opposed to the event-driven algorithm used earlier) for the purposes of improved computational efficiency. Specifically, particle movement is achieved via a hard-particle/overlap technique (Hopkins & Louge 1991). (Note that the simulation results were found to be insensitive to the specific algorithm chosen.) The simulation proceeds by making a series of small time steps, during which the particles are moved along their linear trajectories. After each time step, collisions are detected by searching for overlaps between particles or between a particle and a wall. If an overlap is detected, then the overlap is added to a list of overlaps produced in the given time step. At the end of the time step, the overlap list is inspected for overlaps in excess of 1 % of either particle radius. If an overlap in excess of this distance is detected, then the time step is considered a failure and is reduced by 50 % whereby the new step is taken from the previous point in time. After each successful time step, the collisions are resolved for particles exhibiting overlap. In an effort to resolve the collisions in the correct sequence, the particle–particle collisions and the particle–wall collisions are resolved from largest overlap to smallest overlap. The maximum magnitude of any time step is restricted to the time required for the fastest particle to move a distance equivalent to 40 % of the smallest particles radius. The time step typically employed by the simulation, however, is some fraction of the maximum allowed time step. Over the course of the simulation, the time step is periodically readjusted for efficiency. (For further details, see Dahl & Hrenya 2004)

The input parameters for this simulation are similar to those of the simple shear system, except that the input parameter $\mathrm{d}u_x/\mathrm{d}y$ (shear rate) is no longer relevant and two additional input parameters exist: T_C and T_H, the set values of wall temperature located at $x/L_x = 0$ and $x/L_x = 1$. To establish the temperature gradient, the walls are set to different temperatures with the left-hand wall considered 'cold' (T_C) and the right-hand wall 'hot' (T_H). The dimensionless parameters that describe the system include v, v_1/v_2, d_1/d_2, ρ_{p1}/ρ_{p2}, e, T_H/T_C, L_x/d_1, L_z/L_x and L_y/L_x. The value of L_x/d_1 employed in the simulations is about 15.6. Therefore, a typical simulation (when $v = 0.2$ and $L_z/L_x = L_y/L_x = 1$) has a total number of particles (N) ranging from approximately 1500 to 3600 depending on the values of other simulation parameters (d_1/d_2, v_1/v_2). For all simulations, the periodic domain lengths are set equivalently ($L_y = L_z$). To ensure the simulation results are independent of domain length in the periodic directions, the collected data should not change significantly as the periodic domain lengths are increased. For $L_x/d_1 = 15.6$, a value of $L_z/L_x = L_y/L_x = 1$ ensures such a criterion is met. Specifically, in representative simulations, doubling the values of L_z/L_x and L_y/L_x changes the total solids fraction profile by less than 3 %. As a result, the simulation domain is cubic ($L_x = L_y = L_z$) and the characteristic dimension is hereinafter referred to as L.

A wide parameter space was explored in the context of two-dimensional simulations; however, the focus here is on three dimensions in which a slightly more concentrated parameter space was investigated. Namely, the solids volume fraction (v) was varied between 0.1 and 0.3, the solids volume fraction ratio (v_1/v_2) was set at 1 or 4, the diameter ratio (d_1/d_2) was varied between 1 and 4, the density ratio (ρ_{p1}/ρ_{p2}) was varied between 0.007813 and 4 (m_1/m_2 from 1/16 to 32 for $d_1/d_2 = 2$), the temperature

ratio (T_H/T_C) was set at 10, and the coefficient of restitution (e) was varied between 0.8 and 1. The remaining dimensional quantities, the mass of particle type 1 (m_1) and the domain length (L), were set to 1 for convenience. The outputs from the simulation include lateral profiles of v, v_1, v_2, T_1, T_2 and T.

The simulation proceeds through time until 10 000–20 000 collisions per particle (depending on v) occur before collecting data. At this point, the system has reached a statistical steady state and data collection begins. While there is no bulk flow in the simulation, animations of the system suggest that the local mass-average velocity is non-zero in certain regions. Specifically, the system consists of a fairly dense band of particles near the cold wall that is surrounded by a relatively dilute region. The dense band exhibits a slight oscillatory motion in the lateral direction. This collective motion of particles gives rise to a non-zero local velocity.

A determination of the local mass-average velocity is needed to evaluate the species and mixture granular temperature (since the fluctuation velocity is defined relative to a local mass-average velocity). One method to estimate the mass-average velocity is via local spatial averaging (i.e. averaging over a 'small' region of the domain at a given instant, as was done by Goldhirsch, Tan & Zanetti 1993). For the system under consideration, however, local spatial averaging was found to be inadequate since a 'small' averaging region in the dense region of the domain typically contains a large number of one particle type (the more massive) and few of the other. In the dilute regions, the same-sized region contains few of either particle type. Although an increase in the size of the averaging region is a possible remedy, such an increase was found to smear the lateral variations of interest. Consequently, localized spatial-temporal averaging was pursued (similar to Conway & Glasser 2004). For this averaging method, the characteristic time and length scales used for averaging must be small enough to avoid smearing quantities, but large enough to achieve meaningful averages. For example, a time scale that is too long leads to 'steady-state' values instead of local values (e.g. a zero value for the local mass-average velocity), whereas a time scale that is too short is dominated by noise.

Spatial-temporal averaging was used to quantify all flow-field variables, and was found to be critical in the determination of granular temperature ratio (T_1/T_2) since the granular temperature is defined in terms of the local mass-average velocity. The spatial portion of averaging is accomplished by dividing the domain into small rectangular cells. The size of these cells are determined such that the collected data does not change significantly with further grid resolution. Specifically, the width of the cells is set slightly larger than the root-mean-cube diameter of the particles, and the height and depth are set at twice this value. Doubling the number of divisions causes noise to appear in the total solids fraction profiles. For representative three-dimensional simulations, this grid resolution corresponds to 20 divisions between the constant-temperature walls (x direction) and 10 divisions in both periodic directions (y and z directions). The temporal portion of averaging is achieved by averaging quantities in a given cell over a set number of collisions per particle. The number of collisions per particle averaged over is important, and must be varied across the domain since the characteristic time scale varies across the domain. Further details are discussed in the following section.

During a given temporal averaging period, all flow-field variables are collected at every time step in each spatial cell. After the given temporal period is complete (the specified number of collisions per particle has come to pass), cell averages are calculated and stored, and then the next temporal averaging period begins. Furthermore, the local mass-average velocity calculated during a temporal period is used to

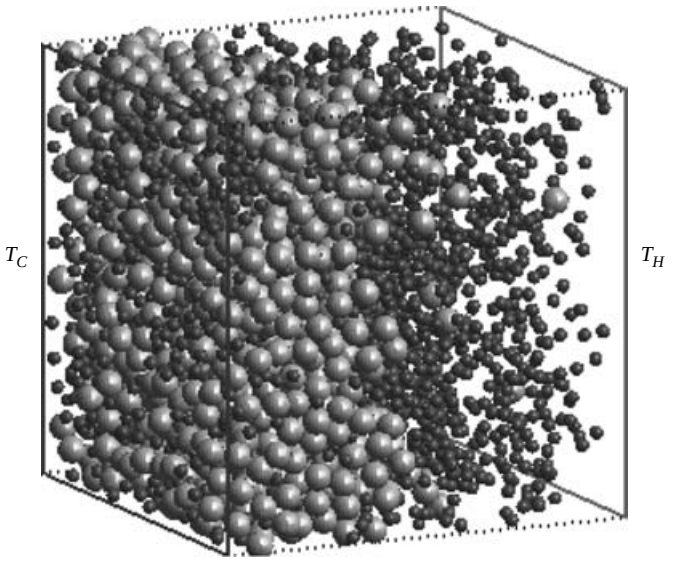

FIGURE 4. Typical snapshot of a simulation consisting of a binary mixture of smooth hard spheres in segregating flow. Relevant parameters: $v = 0.2$, $v_1/v_2 = 4$, $d_1/d_2 = 2$, $\rho_{p1}/\rho_{p2} = 2$ ($m_1/m_2 = 16$), $e = 0.9$, $T_H/T_C = 10$ and $L/d_1 = 15.6$.

calculate the granular temperatures for that period. This process continues until at least 10 000 total collisions per particle have occurred. At this point, the flow variables are reported as a function of x/L by averaging over the boxes in both the y and z directions for all the completed temporal periods.

The solids volume fractions (species and total) within each cell are determined by including the volume of particles whose centre resides in the given data collection region at the instant of measurement. The granular temperatures (species and mixture) are determined similarly to the solids volume fractions. The granular temperatures for each cell (at a given instant) are determined using

$$T_{cell} = \frac{\sum_{j=1}^{n_{cell}} \frac{1}{3} m_j C_{j,cell}^2}{n_{cell}}, \tag{19}$$

where n_{cell} is the number of particles whose centres reside within the data collection region, and $C_{j,cell}$ is the magnitude of the fluctuating velocity of particle j relative to the local mass-average velocities in the cell being considered. For the species granular temperatures, only those associated with the given particle type are considered in the summation, whereas for the mixture granular temperature both particle types are considered.

A statistical steady state is ensured by monitoring both mixture granular temperatures and particle locations (details are given in Dahl & Hrenya 2004).

3.2. *Results and discussion*

In an effort to gauge the influence of a non-equipartition of energy on species segregation, molecular dynamic simulations of the system described in the previous section were performed over a considerable parameter space. The results presented here are from a few representative cases. A snapshot of a typical simulation is presented in figure 4, in which $d_1/d_2 = 2$, and $\rho_{p1}/\rho_{p2} = 2$ ($m_1/m_2 = 16$). Unless otherwise noted,

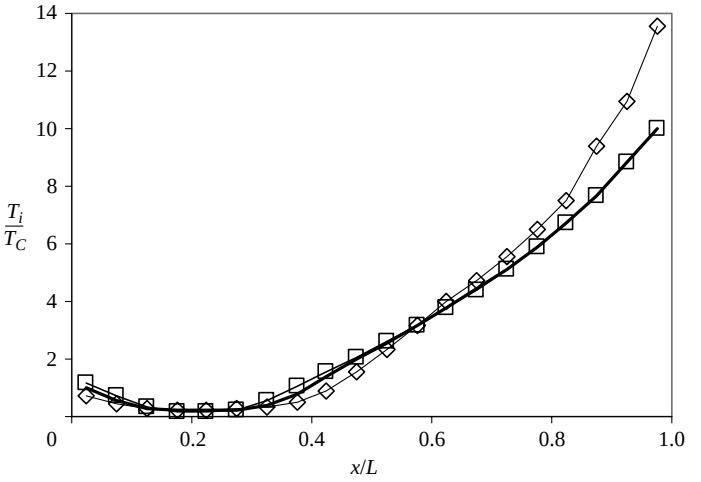

FIGURE 5. Non-dimensional temperature profiles of a binary mixture of smooth hard spheres in segregating flow. MD simulations for species 1 (diamonds), species 2 (squares), mixture (thick solid line). Relevant parameters: $v = 0.2$, $v_1/v_2 = 4$, $d_1/d_2 = 2$, $\rho_{p1}/\rho_{p2} = 2$ ($m_1/m_2 = 16$), $e = 0.9$, $T_H/T_C = 10$ and $L/d_1 = 15.6$.

in this and subsequent diagrams, the simulation parameters are $v = 0.2$, $v_1/v_2 = 4$, $e = 0.9$, $T_H/T_C = 10$ and $L/d_1 = 15.6$. In the following paragraphs, the effect of input parameters on segregation behaviour is overviewed and then followed by an assessment of the relative importance of the various driving forces associated with species segregation.

In the current system, the granular temperature gradient between the two walls drives the segregation process. The resulting dimensionless temperature profiles for the mixture and each particle type are shown in figure 5. All three profiles (T/T_C, T_1/T_C and T_2/T_C) demonstrate nonlinear behaviour between the walls and exhibit a global minimum near the cold wall at $x/L \sim 0.23$. The inelasticity of particle collisions ($e < 1$) serves to dissipate granular energy, which in turn, gives rise to temperatures in the interior of the domain that are less than that of either wall. If the temperature ratio (T_H/T_C) is set to 1, then the global minimum is located at $x/L \sim 0.5$.

A close examination of the dimensionless temperature profile reveals that the observed value of T_H/T_C of 9.9 is different from the set value of T_H/T_C of 10. This deviation is explained by a consideration of how wall temperatures are measured. Namely, the particles in the near-wall region that have already collided with the wall will depart with a granular temperature that, on average, is equal to the set temperature of the wall. However, the particles that are approaching the wall, but have not yet collided, will generally have a smaller granular temperature than the wall (since both walls act as local sources of granular energy). Since the measured granular temperature of the near-wall region includes both departing and approach particles, its value is lower than the set wall temperature.

Under the influence of a granular temperature gradient, the particles display both overall segregation and species segregation. The qualitative nature of this segregation is apparent from the system snapshot shown in figure 4. Evident in the diagram is species segregation. Namely, the larger (more massive) particles tend to concentrate in the coolest region of the domain. The overall segregation exhibited by the system is less apparent owing to the three-dimensional rendering (particles closest to the

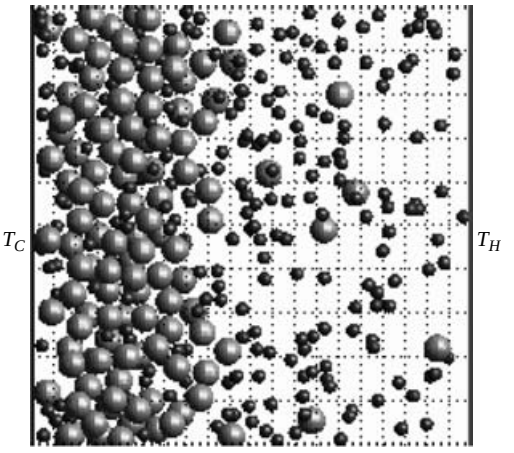

FIGURE 6. A thin slice of a snapshot in the xy-plane at $z/L = 0.5$. Relevant parameters: $v = 0.2$, $v_1/v_2 = 4$, $d_1/d_2 = 2$, $\rho_{p1}/\rho_{p2} = 2$ ($m_1/m_2 = 16$), $e = 0.9$, $T_H/T_C = 10$ and $L/d_1 = 15.6$.

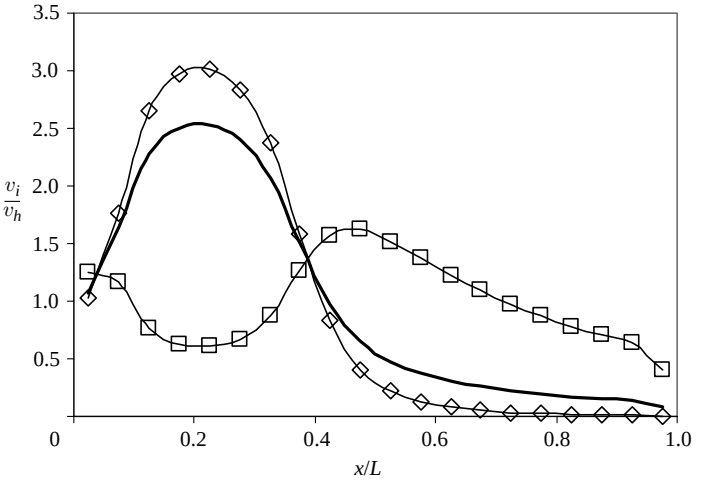

FIGURE 7. Non-dimensional solids volume fraction profiles of a binary mixture of smooth hard spheres in segregating flow. MD simulations for species 1 (diamonds), species 2 (squares), mixture (thick solid line). Relevant parameters: $v = 0.2$, $v_1/v_2 = 4$, $d_1/d_2 = 2$, $\rho_{p1}/\rho_{p2} = 2$ ($m_1/m_2 = 16$), $e = 0.9$, $T_H/T_C = 10$ and $L/d_1 = 15.6$.

viewer can conceal voids and/or particles behind them). To illustrate the degree of overall segregation better, a thin slice of the system in the (x, y)-plane at $z = 0.5$ is also displayed in figure 6.

A quantitative measure of segregation is provided by examining profiles of local solids volume fraction normalized by the solids volume fraction expected if the particles were homogeneously distributed. More specifically, a ratio > 1 indicates a 'particle-rich' region and a ratio < 1 indicates a 'particle-deplete' region, both relative to a uniformly distributed mixture. The corresponding ratios for total solids fraction (v/v_h) and the species solids fractions (v_1/v_{1h} and v_2/v_{2h}) are displayed in figure 7 as a function of the position between the cold and hot walls ($x/L = 0$ and 1, respectively).

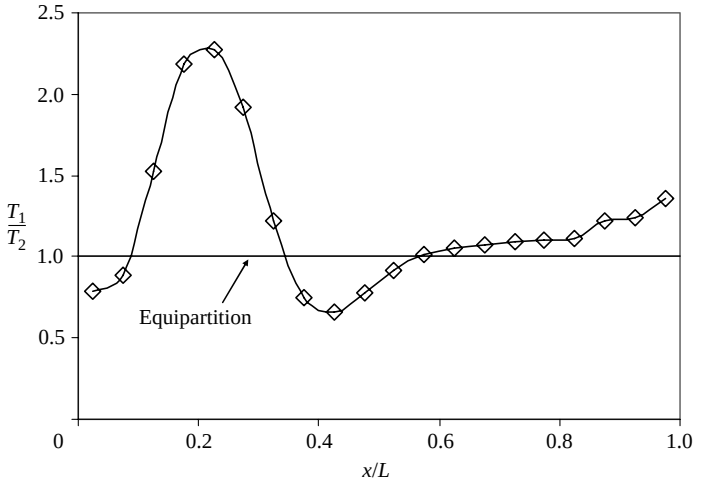

FIGURE 8. Granular temperature ratio of species 1 to species 2 (T_1/T_2). Relevant parameters: $v = 0.2$, $v_1/v_2 = 4$, $d_1/d_2 = 2$, $\rho_{p1}/\rho_{p2} = 2$ ($m_1/m_2 = 16$), $e = 0.9$, $T_H/T_C = 10$ and $L/d_1 = 15.6$.

The v/v_h profile shows the level of overall segregation in the system. An examination of this profile reveals that the particle concentration is highest in the region $x/L \sim 0.23$, where the granular temperature is at a minimum. Correspondingly, the overall particle concentration is fairly dilute in regions of high granular temperature ($x/L > 0.6$). Furthermore, the more massive particles have a greater affinity for the cool region than the less massive particles (i.e. species segregation). For example, the solids fraction of the massive particles is three times greater than would be expected in a homogenous mixture at $x/L = 0.23$ (near the cold wall), but 0.17 times less than would be expected at $x/L = 0.83$ (near the hot wall). In contrast, the solids fraction of the less massive particles demonstrates a minimum at $x/L = 0.23$ and then slowly decreases after $x/L = 0.48$. These observations are in agreement with previous theoretical investigations into thermal diffusion (Hsiau & Hunt 1996; Arnarson & Willits 1998; Louge *et al.* 2000). (The dependencies of overall and species segregation on various input parameters have also been collected during the investigation, but are not included for the sake of brevity.)

Of particular interest in the context of the current investigation is the level of non-equipartition of energy and the relative magnitude of the corresponding non-equipartition driving forces. A close inspection of figure 5 reveals a small disparity in the species granular temperatures. To depict the degree of non-equipartition better, figure 8 displays the granular temperature ratio (T_1/T_2) as a function of x/L. Non-equipartition is greatest near the cold wall, specifically in the region around $x/L = 0.23$ where $T_1/T_2 = 2.3$.

Atypical non-equipartition, namely $T_1/T_2 < 1$, is also found to occur at $x/L \sim 0.43$, which implies that the more massive particle has less granular energy than its lighter counterpart. Although non-equipartition of energy has been observed in numerous theoretical (Garzó & Dufty 1999; Barrat & Trizac 2002; Montanero & Garzó 2003), simulation (Clelland & Hrenya 2002; Dahl *et al.* 2002; Alam & Luding 2003; Paolotti *et al.* 2003) and experimental (Wildman & Parker 2002; Feitosa & Menon 2002) studies, the more massive particle is found to have the greater granular temperature with few exceptions. The theoretical investigation by Barrat & Trizac (2002) considers

the temperature ratio in a non-equilibrium steady state sustained via a stochastic thermostat. They observe T_1/T_2 to be slightly less than 1 for $m_1/m_2 > 1$, but in this case the more massive particle is also more dissipative ($e_{11} < e_{12} < e_{22}$). Feistosa & Menon (2002) report temperature ratios for pairs of different types of grain vibrated in two dimensions. They also observe T_1/T_2 to be slightly less than 1 for m_1/m_2 slightly greater than 1 (aluminium/glass grains) at two different squared vibration velocities, though the error bars overlap with the line $T_1/T_2 = 1$.

A plausible explanation for the unexpected non-equipartition in the current segregating system stems from the likely prior location of particles diffusing to that region. The more massive species are generally concentrated within the dense region of the domain, and the less massive species are more prevalent throughout the dilute region. Furthermore, those particles in the dilute region move freely and possess a higher granular temperature than those in the dense region. A more massive particle leaving the dense region into the dilute region is likely to be involved in collisions with less massive but energetic particles from the dilute region. Consequently, in this region of the domain, the less massive species will have a higher granular temperature than the more massive species. As the more massive particle advances further into the dilute region, subsequent collisions distribute the energy more evenly between species.

The effect of varying input parameters (e, v, m_1/m_2, v_1/v_2, d_1/d_2) on non-equipartition was examined over various parameter spaces. Non-equipartition becomes more prominent with decreasing restitution coefficient, increasing mass disparity and increasing solids volume fraction. Such findings are in agreement with other studies (e.g. Clelland & Hrenya 2002; Alam & Luding 2003) as well as with the simple shear-flow results presented herein. Non-equipartition was also seen to vary with volume fraction ratio, though the behaviour depends on the mass ratio. For systems with $m_1/m_2 > 1$, non-equipartition decreases with increasing solids volume fraction ratio, while for $m_1/m_2 < 1$, non-equipartition increases with increasing solids volume fraction ratio. For $m_1 = m_2$, no significant non-equipartition is observed. The effect of size ratio ($d_1/d_2 = 1$–4) on non-equipartition was also inspected at two different mass ratios ($m_1/m_2 = 1$ and $m_1/m_2 = 4$). For $m_1/m_2 = 4$, no general trends in non-equipartition are observed with increasing diameter ratio. For $m_1/m_2 = 1$, an increase in diameter ratio corresponds to a slight increase in non-equipartition; however, the magnitude of non-equipartition is small in this case (as is consistent with findings of Alam & Luding 2003).

Since the presence of non-equipartition of energy in the segregating system has been established, an examination of the non-equipartition driving forces and their magnitude relative to previously identified driving forces (refer to equation (13)) is warranted. To accomplish this task, the lateral profiles in species number densities (n_1 and n_2), mixture temperature (T) and species temperatures (T_1 and T_2) are obtained from the simulations along with their gradients. The gradients are determined using a second-order centre-difference approximation for the interior grid points and first-order forward- and backward-difference approximations for the wall grid points. The resulting profiles for the flow-field variables and their gradients are then used to approximate the magnitude of each of the driving forces that appear in the diffusion velocity equation (equation (13)). Specifically, each driving force is approximated using the kinetic theory developed by Jenkins & Mancini (1987) (see table 3 for application of Jenkins & Mancini (1987) theory to the system under investigation). This analysis serves as a gauge of the relative magnitude of each of the driving forces since a more complete theory (e.g. non-equipartition, non-Maxwellian and RET) is unavailable.

Granular energy balance: species 1 and species 2

$$\frac{\partial Q_1}{\partial x} = \gamma_1 \quad \frac{\partial Q_2}{\partial x} = \gamma_2$$

Mixture momentum balance

$$\frac{\partial t_{xx}}{\partial x} = 0$$

Diffusion velocity balance

$$0 = -\frac{n^2}{n_1 n_2} D_{12} d_1 = -\frac{n^2}{n_1 n_2} D_{12} \times \left[C_{P1} \frac{\partial P_1}{\partial x} + C_{P2} \frac{\partial P_2}{\partial x} + C_{P1} \frac{\partial P_{new,1}}{\partial x} + C_{P2} \frac{\partial P_{new,2}}{\partial x} + C_{n1} \frac{\partial n_1}{\partial x} + C_{n2} \frac{\partial n_2}{\partial x} + C_T \frac{\partial T}{\partial x} \right]$$

Constitutive relations

$$Q_i = \sum_{k=1,2} q_{ik} = \sum_{k=1,2} g_{ik} r_{ik}^3 \frac{n_i n_k}{m_{ik}} (1+e) T^{3/2} \times \left\{ \begin{array}{l} -\frac{2}{3} r_{ik} \left(\frac{2\pi m_i m_k}{m_{ik}} \right)^{1/2} \frac{\partial \ln(T)}{\partial x} - \frac{m_k}{m_{ik}} (1-e) * \\ \left[\frac{1}{4} r_{ik} (m_k - m_i) \left(\frac{2\pi m_{ik}}{m_i m_k} \right)^{1/2} \frac{\partial \ln(T)}{\partial x} + \frac{1}{6} r_{ik} \left(\frac{2\pi m_{ik}^3}{m_i m_k} \right)^{1/2} \frac{\partial \ln \left(\frac{n_i}{n_k} \right)}{\partial x} \right] \end{array} \right\}$$

$$\gamma_i = 2(1+e) g_{ik} r_{ik}^2 n_i n_k T^{1/2} \left\{ 2 \left(\frac{2\pi m_i m_k}{m_{ik}} \right)^{1/2} \left(\frac{\theta_i - \theta_k}{m_{ik}} \right) - \frac{m_k}{m_{ik}} (1-e) \left(\frac{2\pi m_{ik}}{m_i m_k} \right)^{1/2} \left[T + \frac{3}{2} \left(\frac{m_i \theta_k + m_k \theta_i}{m_{ik}} \right) \right] \right\}$$

$$t_{xx} = \sum_{i=1,2} t_{xx,i} = \sum_{i=1,2} P_i + P_{new,i}$$

$$P_i = \left(n_i + \sum_{k=1,2} K_{ik} \right) T$$

$$P_{new,i} = n_i \theta_i + \sum_{k=1,2} K_{ik} \left(\frac{m_i \theta_k + m_k \theta_i}{m_{ik}} \right)$$

Additional definitions (see table 2 also)

$$C_{P1} = \frac{\rho_2}{\rho n T}, \quad C_{P2} = -\frac{\rho_1}{\rho n T}, \quad C_{n1} = -\frac{K_{12}}{n_1 n}, \quad C_{n2} = \frac{K_{12}}{n_2 n}, \quad C_T = -\frac{K_{12}}{nT} \left(\frac{m_2 - m_1}{m_{12}} \right)$$

$$K_{ik} = \frac{\pi}{3} g_{ik} r_{ik} n_i n_k (1+e)$$

$$D_{ik} = \frac{n_i n_k}{n} \frac{r_{ik}}{K_{ik}} \left(\frac{\pi}{32} \frac{m_{ik}}{m_i m_k} T \right)^{1/2}$$

TABLE 3. Governing equations for segregating flow based on kinetic theory of Jenkins & Mancini (1987). For cases in which the equipartition assumption is imposed, $\theta_1 = \theta_2 = 0$.

The spatial variation of the various driving forces is shown in figure 9 for $v = 0.2$, $v_1/v_2 = 4$, $d_1/d_2 = 2$, $\rho_{p1}/\rho_{p2} = 2$, $e = 0.9$, $T_H/T_C = 10$ and $L/d_1 = 15.6$ (the same parameters as in figures 4–8). An inspection reveals that the larger of the two non-equipartition driving forces is that associated with the less massive species

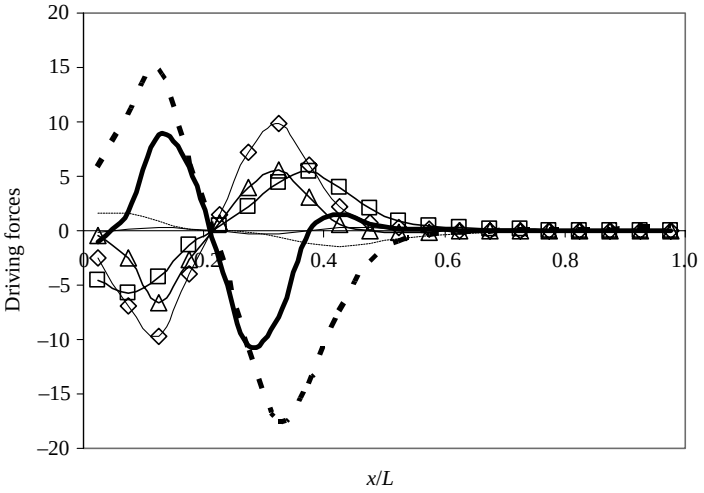

FIGURE 9. Driving forces determined from MD simulations in conjunction with Jenkins & Mancini (1987) theory that are associated with the segregation of a binary mixture of smooth hard spheres. Equipartition driving forces corresponding to $C_{P1}\nabla P_1$ (thin dashed line), $C_{P2}\nabla P_2$ (thick dashed line), $C_{n1}\nabla n_1$ (squares), $C_{n2}\nabla n_2$ (triangles), and $C_T\nabla T$ (diamonds). Non-equipartition driving forces corresponding to $C_{P1}\nabla P_{new,1}$ (thin solid line) and $C_{P2}\nabla P_{new,2}$ (thick solid line). Relevant parameters: $v=0.2$, $v_1/v_2=4$, $d_1/d_2=2$, $\rho_{p1}/\rho_{p2}=2$ ($m_1/m_2=16$), $e=0.9$, $T_H/T_C=10$ and $L/d_1=15.6$.

($C_{P2}\nabla P_{new,2}$). In addition, this non-equipartition driving force ($C_{P2}\nabla P_{new,2}$) is of similar magnitude to the largest remaining driving forces. For example, the maximum magnitude of $C_{P2}\nabla P_{new,2}$ ($C_{P2}\nabla P_{new,2}=8.8$ at $x/L=0.13$) is 59 % as great as the maximum magnitude of the driving force associated with the pressure gradient of species 2 ($C_{P2}\nabla P_2=14.8$ at $x/L=0.13$), which is the largest driving force in this system. Furthermore, the maximum magnitude in $C_{P2}\nabla P_{new,2}$ is 91 % as great as the maximum magnitude of the driving force associated with the mixture temperature gradient ($C_T\nabla T=9.7$ at $x/L=0.13$), which is the next largest driving force. Note that as the level of non-equipartition decreases ($T_1/T_2\rightarrow 1$) the non-equipartition driving forces decrease relative to the other driving forces (figure not shown). (Recall that the temperature ratio approaches unity as the restitution coefficient increases or as the mass ratio nears unity.)

As mentioned earlier, the value of the time scale (number of collisions per particle averaged over in a given cell) used in spatial-temporal averaging is important in the determination of granular temperature and thus the temperature ratio (figure 8). For a given simulation, the time scale used for averaging was varied across the domain based on two criteria. The first criterion requires that the time scale is great enough so, on average, at least 10 'unique' measurements associated with each species in a given cell are made. Since a measurement is made at every time step, a unique measurement refers to a particle that has been involved in a collision or a particle that has entered the cell during a temporal period (as opposed to a particle that has an identical velocity between consecutive time steps in the same cell). The second criterion requires that the time scale is small enough to capture 'instantaneous' (local in time) behaviour as opposed to averaging over these variations. The latter criterion is achieved by first monitoring the local mass average velocity per cell over the course of the simulation for various time scales at various x/L. Based on the examination, an

appropriate time scale is chosen for the corresponding region to ensure a meaningful (noise-reduced) and local (non-smeared) average. As a result, several different time scales are required in the x-direction. In general, the cool region of the domain ($x/L < \sim 0.4$) and the hot region of the domain ($x/L > \sim 0.6$) necessitate a short and long time scale, respectively. The portion of the domain between these two regions calls for the use of several intermediate time scales. (Specifically, four time scales are used between $x/L = 0.4$ and 0.6).

This analysis was implemented for simulation parameters corresponding to those in figures 5–9. The associated time scales for this particular simulation are as follows: 5 collisions/particle for x/L from 0.0 to 0.4 (cool region); 10, 25, 50 and 100 collisions/particle for x/L from 0.4 to 0.45, 0.45 to 0.5, 0.5 to 0.55 and 0.55 to 0.6 (intermediate region), respectively; and 1000 collisions/particle for x/L from 0.6 to 1.0 (hot region) owing to the extremely small number of massive particles in this region.

Several items are worth mentioning at this point. Over a limited region of the domain, the temperature profiles are sensitive to the value of the time scale, whereas the particle concentration profiles are not sensitive to the time scale anywhere in the domain. Specifically, the effects of the time scale on the temperature profiles are most noticeable when short time scales are employed over the hot region of the domain ($x/L > \sim 0.6$). In this case, the temperature of the more massive species suffers from lack of measurements as the number of massive particles radically decreases immediately outside the concentrated region and in the direction of the hot wall. Consequently, the temperature of the more massive species begins to decrease and correspondingly the temperature ratio decreases below unity (where, in this instance, the ratio refers to the massive species temperature over the light species temperature). From a physical standpoint a long time scale is appropriate in the dilute region of the domain since local, collective behaviour is not apparent (as it is in the dense region). In comparison to the hot region of the domain, the averaging results in the cool region are not as sensitive to the value of the time scale. Furthermore, in the cool region of the domain the first criterion (10 unique measurements) is readily obtained with short time scales. In addition, using long time scales in this region has only a slight effect on the temperature ratio profile. Specifically, an increase in the time scale (equivalently, the local mass-average velocity approaches zero) corresponds to a small decrease in the maximum of the temperature ratio profile (at $x/L \sim 0.23$). For example, for a time scale of 5 and 100 collisions per particle the maximum value in the T_1/T_2 profile reduces from 2.3 to 2.0, respectively.

A careful time-scale analysis was pursued to ensure the validity of two major findings: the relative magnitude of the driving forces and the atypical non-equipartition behaviour. Since the driving forces are most significant in the cool region of the domain (figure 9), it is important to have an accurate measurement of the flow parameters in this region. As just noted, however, the temperature profiles are only mildly sensitive to the time scale in this region of the domain. Furthermore, the concentration profiles are insensitive to the time scale. As a result, the exact value of the time scale used for averaging does not affect the observations concerning the relative magnitude of the driving forces. The effect of the time scale on the atypical behaviour of the temperature ratio profile, namely $T_1/T_2 < 1$ for $m_1/m_2 > 1$, was also investigated. The analysis indicates that the $T_1/T_2 < 1$ in the region $0.38 < x/L < 0.60$ is essentially insensitive to the time scale. However, if the chosen time scale in the region $x/L > 0.6$ is made unrealistically small, then the T_1/T_2 ratio will not return to a value greater than unity.

4. Summary

Of the three differences common to kinetic theories of mixtures (and specifically those theories which are based on an assumed form of the velocity distribution), the need to include a non-Maxwellian velocity distribution is well established. As part of the current work, the implications of an equipartition-of-energy assumption have been further explored. Although a significant non-equipartition between unlike particle types is often present, invoking the equipartition assumption does not appear to have detrimental effects on the prediction of the stress tensor in simple shear flow. Nevertheless, for a more complex system in which size and/or density segregation may occur, an analysis of the diffusion-velocity equation (as derived from the Jenkins & Mancini (1987) theory) reveals that non-equipartition leads to additional driving forces for segregation involving $\nabla\theta_1$ and $\nabla\theta_2$ (where θ refers to the difference between species and mixture temperatures; i.e. level of non-equipartition). Molecular-dynamics simulations were used in conjunction with the kinetic theory of Jenkins & Mancini (1987) to estimate the relative magnitude of all driving forces. The results indicate that at least one of the two non-equipartition driving forces is comparable to the largest of the other driving forces present in systems characterized by moderate values of mass ratios and restitution coefficients. Note that this analysis serves as a gauge of the relative magnitude of the driving forces. A better estimate would require a theory that incorporates non-equipartition of energy, a non-Maxwellian velocity distribution, and RET; no such theory, however, is currently available. A similar finding on differences arising from SET versus RET treatments has also been documented. Namely, previous investigators (Arnarson & Jenkins 2000) have shown how the different treatments lead to a different diffusion force, though the impact of such differences on realistic situations has yet to be ascertained. Moreover, a more rigorous estimate of the influence of non-equipartition on segregation would be possible via a kinetic theory based on a systematic solution of the Enskog equation (i.e. one in which an assumed form of the velocity distribution is not required). Again, however, no such theory is currently available. Collectively, these results point to the need for a more elaborate theory that includes non-equipartition effects in order to improve the analysis of segregating systems.

From a practical standpoint, the implications of non-equipartition effects go beyond the added level of complexity of the constitutive relations. In particular, because the inclusion of non-equipartition effects mandates a multi-temperature theory (whereas the equipartition assumption leads to a single-temperature theory), the number of governing equations is larger than in the equipartition counterpart. Accordingly, the computational overhead associated with the numerical solution of the governing equations is higher for the system described according to a non-equipartition of energy. For complex systems, such as three-dimensional dynamical flows, the difference in computational requirements can be substantial. This difference becomes even greater as the number of unlike species increases (since N species energy balances are required for N species). An optimum theory is one capable of providing sufficiently accurate predictions without unnecessary complexities. Accordingly, a theory incorporating non-equipartition of energy seems unnecessary for simple shear flow. However, for more complicated flows (i.e. segregating flows), the results discussed herein point to the need of theoretical models that allow for a non-equipartition of granular energy. An equipartition model is probably sufficient for systems that are nearly elastic or have small mass disparities, otherwise, a non-equipartition model is required.

Finally, an unexpected behaviour has been noted with regard to the temperature ratio in the segregating system. Specifically, within a limited region of the domain, the

less massive species possesses a higher granular temperature than the more massive species. A plausible rationalization for this behaviour is based on the granular temperature in the region from which the majority of particles are diffusing. In particular, in the transitional zone between the dilute and dense regions, the majority of massive particles are expected to diffuse from the lower-temperature dense region, whereas the majority of lighter particles are expected to diffuse from the higher-temperature dilute region.

The authors would like to thank Professor Ben Glasser for sharing his insights on averaging techniques. The authors are grateful to the American Chemical Society Petroleum Research Fund for providing funding for this work (ACS PRF 38065-AC9), as well as to the National Science Foundation and Department of Education (GAANN Program Grant P200A980454) for graduate fellowships provided to S. R. D. (NSF and DoEd) and J. E. G. (DoEd).

REFERENCES

Alam, M. & Luding, S. 2003 Rheology of bidisperse granular mixtures via event-driven simulations. *J. Fluid Mech.* **476**, 69.

Arnarson, B. O. & Jenkins, J. T. 2000 Particle segregation in the context of species momentum balances. *Traffic and Granular Flow '99: Social, Traffic, and Granular Dynamics*. Springer, Berlin.

Arnarson, B. O. & Willits, J. T. 1998 Thermal diffusion in binary mixtures of smooth, nearly elastic spheres with and without gravity. *Phys. Fluids* **10**, 1324.

Barrat, A. & Trizac, E. 2002 Lack of energy equipartition in homogeneous heated binary granular mixtures. *Gran. Matter* **4**, 57.

van Beijeren, H. & Ernst, M. H. 1973 The modified Enskog equation. *Physica* **68**, 437.

Brey, J. J., Cubero, D. & Ruiz-Montero, M. J. 1999 High energy tail in the velocity distribution of a granular gas. *Phys. Rev.* E **59**, 1256.

Bridgwater, J. 1994 Mixing and segregation mechanisms in particle flow. *Granular Matter: An Interdisciplinary Approach*, p. 161. Springer.

Campbell, C. S. 1990 Rapid granular flows. *Annu. Rev. Fluid Mech.* **22**, 57.

Chapman, S. & Cowling, T. G. 1970 *The Mathematical Theory of Non-Uniform Gases*. Cambridge University Press.

Clelland, R. & Hrenya, C. M. 2002 Simulations of a binary-sized mixture of inelastic grains in rapid shear flow. *Phys. Rev.* E **65**, 031301.

Conway, S. L. & Glasser, B. J. 2004 Density waves and coherent structures in granular Couette flows. *Phys. Fluids* **16**, 509.

Dahl, S. R., Clelland, R. & Hrenya, C. M. 2002 The effects of continuous size distributions on the rapid flow of inelastic particles. *Phys. Fluids* **14**, 1972.

Dahl, S. R. & Hrenya, C. M. 2004 Size segregation in rapid, granular flows with continuous size distributions. *Phys. Fluids* **16**, 1.

Ernst, M. H. 2000 Kinetic theory of granular fluids: hard and soft inelastic spheres. *Dynamics: Models and Kinetic Methods for Non-equilibrium Many Body Systems*, p. 239. Kluwer.

Esipov, S. E. & Pöschel, T. 1997 The granular phase diagram. *J. Stat. Phys.* **86**, 1385.

Feitosa, K. & Menon, N. 2002 Breakdown of energy equipartition in a 2D binary vibrated granular gas. *Phys. Rev. Lett.* **88**, 198301.

Garzó, V. & Dufty, J. 1999 Homogeneous cooling state for a granular mixture. *Phys. Rev.* E **60**, 5706.

Garzó, V. & Dufty, J. W. 2002 Hydrodynamics for a granular binary mixture at low density. *Phys. Fluids* **14**, 1476.

Goldhirsch, I. 2003 Rapid granular flows. *Annu. Rev. Fluid Mech.* **35**, 267.

Goldhirsch, I. & Tan, M.-L. 1996 The single-particle distribution function for rapid granular shear flows of smooth inelastic disks. *Phys. Fluids* **8**, 1752.

Goldhirsch, I., Tan, M.-L. & Zanetti, G. 1993 A molecular dynamical study of granular fluids. I: The unforced granular gas in two dimensions. *J. Sci. Comput.* **8**, 1.

Goldshtein, A. & Shapiro, M. 1995 Mechanics of collisional motion of granular materials. Part 1. General hydrodynamic equations. *J. Fluid Mech.* **282**, 75.

Hopkins, M. & Louge, M. 1991 Inelastic microstructure in rapid granular flows of smooth disks. *Phys. Fluids* A **3**, 47.

Hsiau, S. S. & Hunt, M. L. 1996 Granular thermal diffusion in flows of binary-sized mixtures. *Acta Mech.* **114**, 121.

Huilin, L., Gidaspow, D. & Manger, E. 2001 Kinetic theory of fluidized binary granular mixtures. *Phys. Rev.* E **64**, 061301.

Jenkins, J. T. 1998 Particle segregation in collisional flows of inelastic spheres. *Physics of Dry Granular Media*, p. 645. Kluwer.

Jenkins, J. T. & Mancini, F. 1987 Balance laws and constitutive relations for plane flows of a dense, binary mixture of smooth, nearly elastic, circular disks. *J. Appl. Mech.* **54**, 27.

Jenkins, J. T. & Mancini, F. 1989 Kinetic theory for binary mixtures of smooth, nearly elastic spheres. *Phys. Fluids* A **1**, 2050.

Khakhar, D. V., McCarthy, J. J. & Ottino, J. M. 1999 Mixing and segregation of granular materials in chute flows. *Chaos* **9**, 594.

Kudrolli, A. & Henry, J. 2000 Non-Gaussian velocity distributions in excited granular matter in the absence of clustering. *Phys. Rev.* E **62**, 1489.

Losert, W., Cooper, D. G. W., Delour, J., Kudrolli, A. & Gollub, J. P. 1999 Velocity statistics in excited granular media. *Chaos* **9**, 682.

Louge, M., Jenkins, J., Xu, H. & Arnarson, B. 2001 Granular segregation in collisional shearing flows. *Mechanics for a New Millennium*, p. 239. Kluwer.

Louge, M. Y., Jenkins, J. T., Reeves, A. & Keast, S. 2000 Microgravity segregation in collisional granular shearing flows. *IUTAM Symp. on Segregation in Granular Flows*, p. 103. Kluwer.

Luding, S., Strauss, O. & McNamara, S. 2000 Segregation of polydisperse granular media in the presence of a temperature gradient. *IUTAM Symp. on Segregation in Granular Flows*. Kluwer.

Montanero, J. M. & Garzó, V. 2003 Energy nonequipartition in a sheared granular mixture. *Mol. Sim.* **29**, 357.

van Noije, T. P. C. & Ernst, M. H. 1998 Velocity distributions in homogeneous granular fluids: the free and heated case. *Granular Matter* **1**, 57.

Ottino, J. M. & Khakhar, D. V. 2000 Mixing and segregation of granular materials. *Annu. Rev. Fluid Mech.* **32**, 55.

Paolotti, D., Cattuto, C., Marconi, U. M. B. & Puglisi, A. 2003 Dynamical properties of vibrofluidized granular mixtures. *Granular Matter* **5**, 75.

Press, W. H., Flannery, B. P., Teukolsky, S. A. & Vetterling, W. T. 1992 *Numerical Recipes in C: The Art of Scientific Computing*. Cambridge University Press.

Rahaman, M. F., Naser, J. & Witt, P. J. 2003 An unequal temperature kinetic theory: description of granular flow with multiple particle classes. *Powder Tech.* **138**, 82.

Rosato, A. D. & Blackmore, D. L. (ed.) 2000 *IUTAM Symp. on Segregation in Granular Flows*. Kluwer.

Savage, S. B. 1987 Interparticle percolation and segregation in granular materials: a review. *Developments in Engineering Mechanics*, p. 347. Elsevier.

Tan, M.-L. & Goldhirsch, I. 1997 Intercluster Interactions in rapid granular shear flows. *Phys. Fluids* **9**, 856.

Wildman, R. D. & Parker, D. J. 2002 Coexistence of two granular temperatures in binary vibrofluidized beds. *Phys. Rev. Lett.* **88**, 064301.

Willits, J. T. & Arnarson, B. O. 1999 Kinetic theory of a binary mixture of nearly elastic disks. *Phys. Fluids* **11**, 3116.

Zamankhan, P. 1995 Kinetic theory of multicomponent mixtures of slightly inelastic spherical particles. *Phys. Rev.* E **52**, 4877.